ABSTRACT

Simulation Studies of the Time Digitizer for the CMS Hadron Calorimeter Upgrade

Evan Bauer

Director: Kenichi Hatakeyama, Ph.D.

The Large Hadron Collider (LHC) has performed exceptionally well so far, delivering more than 10^{15} proton-proton collisions with center-of-mass energy up to 8 TeV. It has already provided the data that enabled the CMS and ATLAS experiments to announce discovery of the Higgs boson, but the LHC is still far from achieving its full potential. The LHC will be upgraded in 2013–2014 in order to provide higher energy collisions at higher luminosities, and the Compact Muon Solenoid (CMS) detector must be upgraded in the coming years to take full advantage of this LHC upgrade. As part of this upgrade to CMS, new electronics have been proposed for readout of the CMS hadron calorimeter, including a time digitizer component known as the Time-to-Digital Converter (TDC) that provides high-resolution time information. This thesis investigates simulations of the upgraded CMS detector in order to gain a better understanding of the TDC functionality in the upgraded CMS configuration. These simulations enable calibration of TDC-based timing information, and they reveal that the timing resolution gained through this calibration makes it possible to reject key backgrounds. The advantages of this background rejection provide strong motivation for the proposed upgrades to the CMS detector.

APPROVED BY DIRECTOR OF HONORS THESIS:

_____

Dr. Kenichi Hatakeyama, Department of Physics

APPROVED BY THE HONORS PROGRAM:

_____

Dr. Andrew Wisely, Director

DATE: _____

SIMULATION STUDIES OF THE TIME DIGITIZER FOR THE CMS HADRON CALORIMETER UPGRADE

A Thesis Submitted to the Faculty of

Baylor University

In Partial Fulfillment of the Requirements for the

Honors Program

By

Evan Bauer

Waco, Texas

May 2013

TABLE OF CONTENTS

LIST OF FIGURES

LIST OF TABLES

ACKNOWLEDGMENTS

I would like to thank the Baylor University physics department for encouraging and facilitating undergraduate research at all the various stages of this work. In particular, I want to express my gratitude to Dr. Jay Dittmann, who stimulated my interest in physics when I first came to Baylor and provided my first contact with the Baylor HEP group with which I ended up working. I especially want to thank my advisor, Dr. Kenichi Hatakeyama, who dedicated countless hours to teaching and mentoring me through this process. This project simply would not have happened without his constant involvement, and I am truly grateful for the many things he has taught me. I would also like to thank the other two readers on my committee, Dr. David Ryden and Dr. Zhenrong Zhang. I appreciate the interest they expressed and the thoughtful questions they brought up that suggested improvements.

The Baylor University Honors Program has been a great encouragement through this process as well. I am particularly thankful for the guidance received from Dr. Al Beck and Diane Haun. Their general wisdom and experience with the honors thesis process was quite valuable in approaching aspects of the project like formatting and overall structure. Finally, I would like to acknowledge the United States Department of Energy, which provided much of the funding for the research presented in this thesis.

CHAPTER ONE

Introduction

"Even the so-called elements are shifting." — Ovid, *Metamorphoses*

It seems that as long as humans have existed, we have wondered on some level what matter is made of. Philosophers and scientists have sought to understand the "elements" of which matter is composed. This search has progressed from philosophical debates among the ancient Greeks to more empirical attempts by modern scientists. The former wondered whether matter was continuous (uniform and infinitely divisible) or discrete (made up of distinct, indivisible particles), and speculated on what substances were truly the fundamental elements of all matter. Many Greek philosophers followed Democritus in claiming that matter was indeed discrete, composed of fundamental building blocks called atoms, though they lacked the ability to study these tiny particles empirically, and what we call atoms today are known to be composed of yet smaller particles.

More recently, a great deal of success has been achieved in measuring and quantifying the particles that seem to be the building blocks for the matter around us. Most of the particles that comprise ordinary matter are now understood at an extraordinary level of detail. Yet the question remains of whether these particles are truly fundamental or further divisible. More importantly, the framework that provides such exceptional understanding of these ordinary elementary particles also allows for a vast number of other, more exotic particles, completely different from the matter that constitutes the atoms encountered in everyday experience. Many of these particles have also been discovered and studied (see Sections 1.1 and 1.2 on elementary particles and the standard model), but some compelling theories suggest the existence of more particles that have yet to be detected (see Section 1.3 on

supersymmetry). Gaining empirical data on some of these hypothetical particles may provide important explanations for unsolved questions on what the universe is made of and how it works.

Many of the elementary particles that have been the subject of recent research are in some sense quite rare, because they are inherently unstable and decay into more stable particles after extremely short periods of time. This makes it very challenging to find and detect the interesting particles that we wish to study. Some of these particles are provided by the cosmic rays that constantly bombard the earth from space, so early particle physics efforts relied on these cosmic rays for data collection. Cosmic sources, however, offer limited potential for collecting large amounts of data, which can be essential for studies of certain types of particles, and this eventually motivated more involved methods of producing elementary particles. The most common tools for producing elementary particles today are high-energy particle accelerators, which collide particles such as protons or electrons at very high energy scales. The enormous energies released in these head-on collisions can produce large numbers of elementary particles, and the challenge at that point is detecting the collision products.

The particles we tend to search for are minute, smaller than atoms, so processes for detection are never simple. Methods of detection have grown increasingly complex over the past century in order to cope with the increasing demands of probing fundamental particle physics. Detector apparatuses have employed progressively more complicated equipment over the years, from relatively simple cloud chambers, spark chambers, and bubble chambers to the much more involved devices used in modern experiments. One such modern-day apparatus is the Compact Muon Solenoid (CMS), which integrates many different advanced detection technologies. Thousands of physicists from all over the world are involved in analyzing the data collected from CMS, many of whom are experts specifically in the design,

upkeep, and upgrades for the detector apparatus. This last category, upgrades to CMS, is the primary concern of this thesis, and these upgrades will be discussed at length in subsequent chapters, following the more detailed description of our current knowledge of elementary particles in the remainder of this chapter. Hopefully, these upgrades to CMS will provide detection capabilities that lead to even more exciting discoveries in the field of elementary particle physics, shifting our understanding of the so-called "elements" once again.

1.1 Elementary Particles

For many people, when they hear about "elementary" or "fundamental" particles, they think of the elements occupying the periodic table. These atoms are important for considering the discrete nature of matter and studying its chemical properties, but we now know that atoms are at least a few steps away from being truly elementary. They are composed of constituent parts, namely electrons, protons, and neutrons. Protons and neutrons are in turn composed of collections of smaller particles called quarks, while electrons are currently thought to be truly fundamental. So which particles form the set of truly elementary particles, and how do we classify them?

During the 19th century, physicists sought to understand quantization of electric charge, and in 1897 J.J. Thomson's now famous experiment demonstrated that this charge was carried by small particles with negative charge, dubbed electrons. It was also discovered that these electrons could be separated from atoms, showing that they were constituent parts of atoms. For some time, it was thought that these negatively charged electrons floated in a positive sea, yielding atoms with net neutral charge, but Ernest Rutherford's scattering experiments in 1911 showed that the positive charge and most of the atomic mass is concentrated in a dense nucleus. The positively charged particles residing in this nucleus became known as protons,

while another class of neutral particles also found in the nucleus became known as neutrons.

Protons, neutrons, and electrons together account for the structure of all of the elements on the periodic table, and hence all of the familiar matter which we encounter every day. However, as experimental techniques progressed in the 20th century, discoveries of other new particles proliferated. Many of these new particles exhibited properties similar to protons and neutrons, though their masses could be much larger. This class of particles became known as hadrons, and so many were discovered that theory and experiment began to point to a smaller group of more elementary particles of which these hadrons are composed. Still other particles were discovered that behaved more like electrons than hadrons, and these are thought to be fundamental in their own right. Currently, elementary particles are classified into three groups: leptons (like the electron), quarks (the particles that make up protons, neutrons, and other hadrons), and gauge bosons [1].

The class of leptons contains six particles, organized into three generations. The first generation contains the electron and its associated neutrino. Discovered somewhat later, the muon and its associated neutrino comprise the second generation. The third generation contains the tau lepton and its associated neutrino. These leptons each carry integral charge (with respect to the units of fundamental electric charge, e), with that integer being 0 for neutrinos and –1 for other leptons. The three neutrinos were long thought to be massless, but more recent experiments on neutrino flavor oscillation have indicated that they have finite mass, though this mass is nearly negligible, much less than even the electron mass. The other leptons grow successively more massive with each generation, with the muon hundreds of times more massive than the electron, and the tau another order of magnitude beyond the muon mass (see Table 1.1 for exact values).

The class of quarks also contains six particles organized into three generations, with up and down in the first generation, charm and strange in the second, and top and bottom in the third. Unlike leptons, quarks carry fractional charge, but they must exist in states bound with other quarks in such a way that the resulting composite particle always possesses integral charge, so fractional charge is never directly observed in nature. The masses of quarks also increase with generation, though this can be hard to measure due to the complicated structure of the particles in which they are bound. The quark model was proposed in the 1960's and encountered a great deal of success explaining hadrons, but the last of the six known quarks, the top, was not discovered until 1995 due to its large mass, which is comparable to the mass of an entire gold atom. The discovery of the top quark was one of the greatest successes of the Tevatron proton-antiproton collider and associated experiments at Fermilab. The bound states in which we observe quarks are the previously mentioned hadrons, and these come in two varieties: mesons and baryons.[1] Mesons are composed of just two quarks, while baryons are composed of three. The familiar protons and neutrons are both baryons, but pions and other mesons are also quite commonly encountered in the realm of experimental high-energy physics.

The last group of elementary particles, gauge bosons, contains four particles thought to mediate the fundamental forces of nature. These four force carriers are the gluon, the $W^{\pm}$, the Z^0, and the photon. The $W^{\pm}$ carries charge, but the others are neutral. The photon and gluon are massless, while the $W^{\pm}$ and Z^0 carry mass. The 16 particles described above are summarized along with their basic properties in Table 1.1. It should be noted that the lighter quarks present a challenge for measurement and interpretation of their masses since they are impossible to isolate, and unlike other quarks their masses turn out to be much smaller than the binding

[1] Technically, the top quark should be excluded from a discussion of hadrons because it is too massive and decays too quickly to bind with other particles and form hadrons.

Table 1.1: Standard model particles (Charge is given in units of the elementary charge e, equal to the absolute value of the electron charge. Mass values obtained from the *Review of Particle Physics* [2].)

	Generation	Particle	Charge	Mass (MeV/c^2)
Leptons	First	e (electron)	–1	0.511
		ν_e (e neutrino)	0	≈ 0
	Second	μ (muon)	–1	105.658
		ν_μ (μ neutrino)	0	≈ 0
	Third	τ (tau)	–1	1776.82
		ν_τ (τ neutrino)	0	≈ 0
Quarks	First	d (down)	–1/3	4.8
		u (up)	2/3	2.3
	Second	s (strange)	–1/3	95
		c (charm)	2/3	1275
	Third	b (bottom)	–1/3	4180
		t (top)	2/3	173500
Gauge Bosons		g (gluon)	0	0
		γ (photon)	0	0
		$W^\pm$	± 1	80385
		Z^0	0	91187

energies of the hadrons in which they are bound, so their masses given in the table are only approximate.

No description of elementary particles would be complete without mention of antiparticles. For each of the leptons, quarks, and bosons discussed above, an antiparticle exists with the same mass but opposite charge. For example, the antiparticle of the electron is the positron, which carries positive charge equal in magnitude to the electron's. A neutral particle like the photon can be its own antiparticle, though this is not always the case. For example, the antineutron is composed of antiquarks rather than quarks, so it is distinct from the neutron, though both are neutral.

1.2 The Standard Model

The goal of high-energy physics is not only to find elementary particles, but also to understand the fundamental forces which govern their interactions. These forces can be described in terms of four categories: gravity, electromagnetism, strong nuclear, and weak nuclear. Gravity has been studied for hundreds of years because of its macroscopic scale effects, and Einstein's theory of relativity provides the framework for modern understanding of gravity. The other three fundamental forces are much more important for understanding the much smaller-scale interactions of elementary particles, and the standard model provides the theoretical framework for understanding each of these other three forces. The standard model has been very successful over the years in explaining and predicting the existence of fundamental particles and their interactions. It describes each of the fundamental forces as an interaction mediated by one of the previously mentioned gauge bosons.

Quantum Electrodynamics (QED) is the aspect of the standard model dealing with the electromagnetic force. Electromagnetic interactions occur between charged particles, mediated by the photon according to QED. In the macroscopic world, QED reduces to the familiar electromagnetic theory developed in the 19th century, but QED is also quite successful in describing more subtle physical phenomena at the quantum level.

The strong nuclear force is also mediated by a massless gauge boson, the gluon, but the interactions due to this force are even more complicated than those in QED. Strong force interactions are described in terms of "colors," which are exchanged via gluons. Hence, the theory governing these interactions is known as Quantum Chromodynamics (QCD), though the "colors" used to describe them do not correspond to a physical phenomenon related to the visible color spectrum. Rather, these colors are convenient representations for the mathematical structure of the underlying symmetries that can be expressed more formally in group theory.

Quarks carry color and must form bound states with color that mixes to form white. The resulting hadrons are color neutral, but their constituent quarks must each be a different color to account for this neutrality. Gluons carry color between quarks as their exchange mediates strong force interactions.

In the standard model, electroweak theory provides a unified theory to describe both electromagnetic and weak force interactions. The details of this unification are quite involved, beyond the scope of this thesis, but it is worth noting a few consequences of this electroweak theory. To begin, it describes weak interactions which are mediated by the massive $W^{\pm}$ and Z^0 bosons. In fact, at the time it was posited, it predicted the existence of these particles, which had yet to be observed. Their eventual discovery and measurement at CERN in the 1980's marked a major success for this theory and confirmation of its strong predictive power. One other important aspect of the electroweak theory is that the $W^{\pm}$ and Z^0 bosons acquire their high masses through the Higgs mechanism, while the photon stays massless. Along with the Higgs mechanism came at least one new predicted particle, the Higgs boson, which also gives masses to quarks and leptons through their Yukawa couplings. Because of the incredible success of electroweak theory in other areas, many physicists believed in the theoretical validity of the Higgs mechanism and the existence of the Higgs boson for years before finally finding direct experimental evidence that such a particle indeed exists. The Higgs boson turned out to be quite massive at around 125 GeV/c^2, part of the reason it was only discovered in 2012 after a gargantuan collaborative effort by the CMS and ATLAS experiments. Among accelerators, only the Tevatron and LHC achieved energies high enough for sensitivity to the Higgs mass region. Careful analysis of data collected from the Tevatron revealed hints of a Higgs at mass 125 GeV/c^2, but data from CMS and ATLAS detectors at the LHC were necessary to provide sufficient evidence to claim discovery.

1.3 Physics Beyond the Standard Model: Supersymmetry

With the recent discovery of the Higgs boson, the standard model is now on very strong footing, but there is still much to explore in the world of elementary particles. A theoretical expansion of the standard model known as supersymmetry has now become one of the most important frontiers of particle physics, as it has the potential to provide compelling explanations for physical phenomena that are still not fully understood. The detectors responsible for the discovery of the Higgs boson at CERN were designed as general-purpose detectors, meaning they should have robust capability to detect all sorts of particle interactions, including those important for supersymmetry searches. As the energy of collisions at the Large Hadron Collider continues to increase, scientists hope that these detectors will begin to see more and more hints of physics beyond the standard model.

What is supersymmetry? It is a theory that proposes a new set of supersymmetric particles in one-to-one correspondence with the known particles of the standard model. Each known standard model particle would thus have a supersymmetric partner. The leptons and quarks belong to a class of particles known as fermions because they have spin 1/2, while the bosons carry spin 1. Supersymmetry proposes that the supersymmetric partners of standard model fermions would be bosons, while the partners of the gauge bosons would be fermions. It is also believed that these supersymmetric particles tend to be much more massive than their standard model partners, so we may only be at the brink of colliders accessing the energies necessary to observe these particles in experiments. None of these particles have yet been observed, but the theory has a great deal of potential if we can gain experimental sensitivity to these particles.

Supersymmetric particles are generally denoted by placing tildes above the symbols for their respective standard model partners. Naming conventions for supersymmetric particles have taken a rather whimsical form. The bosonic super-

partners of standard model fermions are named by placing an "s" at the beginning of their partners' names. Examples of these are "sleptons" such as the the "selectron" ($\tilde{e}$) and "stau" ($\tilde{\tau}$), and "squarks" such as the "stop" ($\tilde{t}$) and "sbottom" ($\tilde{b}$). The fermionic superpartners of gauge bosons are named by adding "ino" to the end of the gauge boson partner name. Known as "gauginos," these are the "bino ($\widetilde{B}^0$), winos ($\widetilde{W}^{\pm}$,$\widetilde{W}^0$), and gluino ($\tilde{g}$)." The supersymmetric partners of the photon and the Z^0, the "photino" ($\tilde{\gamma}$) and "zino" ($\widetilde{Z}^0$), are actually superpositions of the $\widetilde{B}^0$ and $\widetilde{W}^0$ states. Supersymmetry also proposes a few more supersymmetric fermions: the "gravitino" ($\widetilde{G}$) as the partner to the hypothetical graviton (which mediates gravitational interactions) and the "Higgsinos" ($\tilde{h}^0, \widetilde{H}^0, \widetilde{H}^{\pm}, \tilde{A}^0$) as partners of Higgs bosons. The above gauginos are given in terms of the gauge eigenstates of the particles, which govern their force interactions. They can also be categorized according to the mass eigenstates, which are superpositions of the gauge eigenstates. These mass states are the "charginos" ($\tilde{\chi}_1^{\pm}, \tilde{\chi}_2^{\pm}$) and "neutralinos" ($\tilde{\chi}_1^0, \tilde{\chi}_2^0, \tilde{\chi}_3^0, \tilde{\chi}_4^0$). Other terms are often adopted based on these naming conventions, such as "EWKino" (Fig. 1.2) to refer to this collection of gauginos, since they are the supersymmetric partners of the gauge bosons involved with the electroweak force.

Supersymmetry is an important frontier for high-energy physics because of this potential it has for explaining physical phenomena that remain as yet enigmatic. For example, supersymmetry provides a particle that interacts very minimally but is quite massive, and is thus a compelling candidate for explaining the preponderance of dark matter in the universe. No known standard model particle provides nearly as good of an explanation for dark matter, with neutrinos simply being too light, and other particles not being "dark" enough. Another attractive feature of supersymmetry is that it motivates certain modifications to the coupling constants for the three fundamental forces in the standard model, such that they run together at sufficiently high energy scales. This provides a step in the direction of a

so-called "Grand Unified Theory" for fundamental physics, and thus makes finding experimental evidence of supersymmetry a high priority for physicists.

Searches for supersymmetry have been a major part of CMS data analysis since the LHC started running in 2010. So far no significant experimental evidence of supersymmetry has been observed, though this evidence was not necessarily expected with the somewhat conservative energies and luminosities provided by the LHC up to this point. During the summer of 2011, I had the opportunity to participate in one such search for supersymmetry, which was focused on data containing all-hadronic events and missing energy signatures. This all-hadronic analysis found no excess of events above predicted standard model backgrounds, resulting in the conclusion that no signs of supersymmetry were observed. We examined the data within the context of the Constrained Minimal Supersymmetric Standard Model (CMSSM), which is one of the simplest formulations of supersymmetry characterized by two key parameters: the common gaugino mass ($m_{1/2}$) and the common scalar mass (m_0). Using 2011 data, we were able to set limits on these two parameters at the 95% confidence level.[2] Other analyses have since been able to use the data collected after 2011 to push the limits on these parameters even further. Some of these limits are visually represented in Fig. 1.1, which displays the results in a two dimensional m_0–$m_{1/2}$ plane, where any values of (m_0, $m_{1/2}$) that fall below and to the left of the contour are excluded at the 95% confidence level. The plots in Fig. 1.1 also show curves relating gluino and squark masses to the m_0 and $m_{1/2}$ in that plane. These curves show that the search with the full 2011 data excluded the squark masses below 1.2 TeV and gluino masses below 0.72 GeV within the context of CMSSM.

The exclusion contours in Fig. 1.1 motivate upgrades to the LHC and CMS, in order that we might gain sensitivity to the higher mass regions for supersymme-

[2] See Appendix A for more information on CMSSM studies and the statistical methods used for setting these limits.

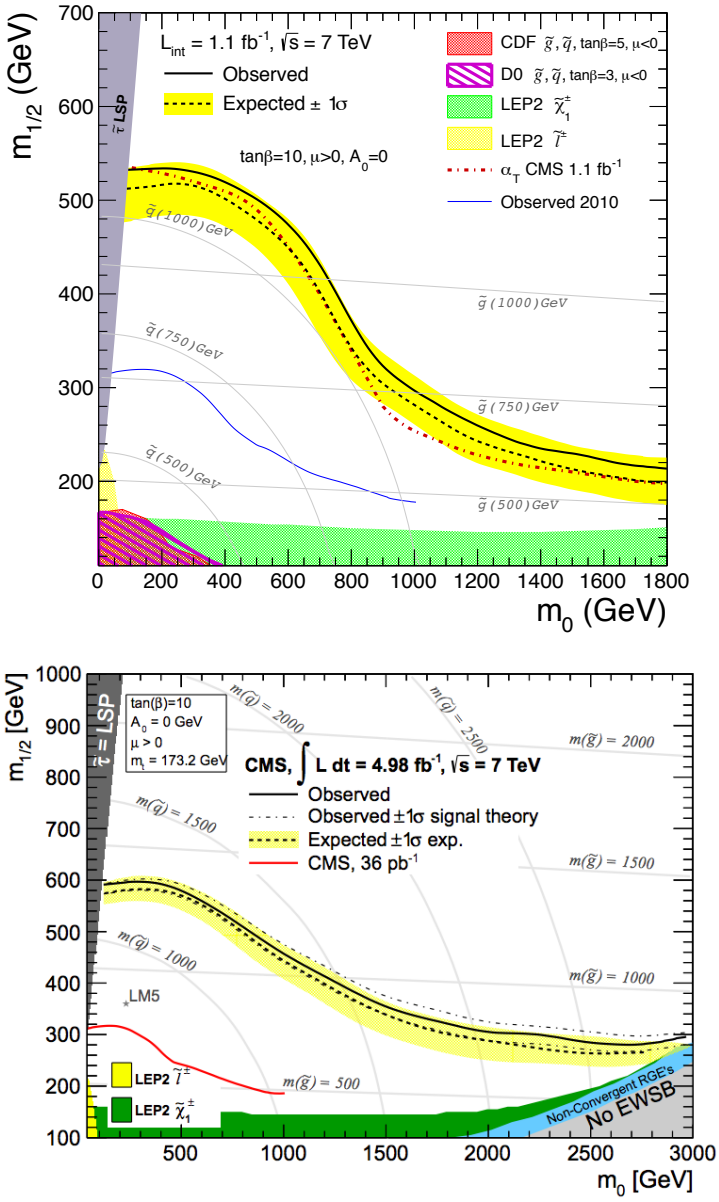

Figure 1.1: The observed and expected 95% confidence level limits in the CMSSM m_0–$m_{1/2}$ plane. The yellow-shaded region shows the $\pm 1\sigma$ variation in the expected limit. The other filled or shaded regions represent areas excluded by previous studies. The top plot is taken from the all-hadronic supersymmetry search in which I participated based on the dataset that was available in August 2011 [3]. The lower plot extends the reach of the exclusion based on a larger dataset available at the end of 2011 [4].

try required by the exclusion of lower ranges from current data. Simply expanding the datasets obtained with the current LHC and CMS configurations may not be sufficient for the discoveries we hope to achieve at the LHC, as data collected from only 7–8 TeV collisions may lack sensitivity to massive supersymmetry particles. Figure 1.2 shows the expected reach of an upgraded LHC that would provide higher energies and luminosities, providing the opportunity to discover particles much more massive than those currently accessible. With an increasingly powerful LHC, detectors such as CMS must be upgraded to keep pace with the data available to them. Thus, supersymmetry is significant for this thesis because it provides motivation for the detector upgrade explored in the remaining chapters. In order to handle the increased amounts of data provided by the LHC at much higher energies, CMS must be upgraded to collect the largest amount of high quality data possible.

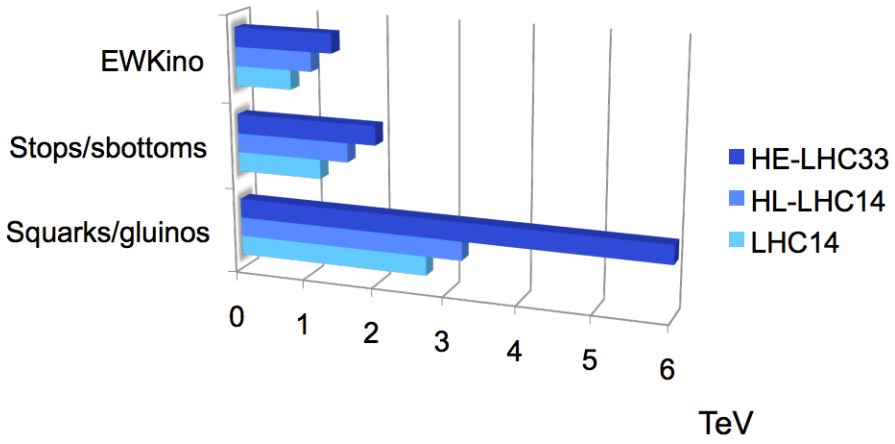

Figure 1.2: Anticipated mass ranges achievable for three different types of supersymmetric particles that could potentially be produced at the LHC. "LHC14" represents 300 fb^{-1} of data collected from collisions at center-of-mass energy 14 TeV. "HL-LHC14" stands for "High Luminosity LHC," which would collect 3000 fb^{-1} of data. "HE-LHC33" stands for "High Energy LHC," collecting 300 fb^{-1} of data at center-of-mass energy 33 TeV. See Section 2.3 for more details on scheduled LHC energy and luminosity.

CHAPTER TWO

Experimental Apparatus: Accelerator, Detectors, and Upgrades

The physics of elementary particles involves a vast collaborative effort on the part of many physicists working in both theoretical and experimental capacities. These physicists are confronted with the challenges of understanding the relationships between known particles and finding ways to detect new elementary particles. How does one go about detecting and discovering these elementary particles? The answer to this question is becoming increasingly complex. Whereas a relatively simple cloud chamber may have sufficed a century ago, the pursuit of today's elusive particles (Higgs bosons, supersymmetric particles) often demands an extremely sophisticated, large scale apparatus. It is just this sort of apparatus that provides both the setting and subject of the research discussed in this thesis, since this research is experimental in nature and involves upgrades to one of the particle detectors at CERN.

A variety of methods exist for producing elementary particles in order to detect them, but many of the most successful methods involve particle accelerators. Many of the particles sought in modern experiments can be quite massive in comparison to the more ordinary fundamental particles such as electrons. Particle accelerators make it possible to produce these massive particles by injecting extremely large amounts of energy into very small amounts of matter. This is accomplished by accelerating particles such as protons to high energies and then colliding them (hence the moniker "high-energy physics"). The fragments of these collisions are not simply pieces of protons, but all sorts of other types of particles as well (other hadrons, photons, and even leptons). Thanks to mass-energy equivalence, the high-energy interactions of colliding protons often lead to the creation of particles much more

massive than the incident protons. By setting up detectors around the collision points at particle accelerators, physicists can collect and analyze data, sometimes leading to the discovery of a new particle.

2.1 The Large Hadron Collider (LHC)

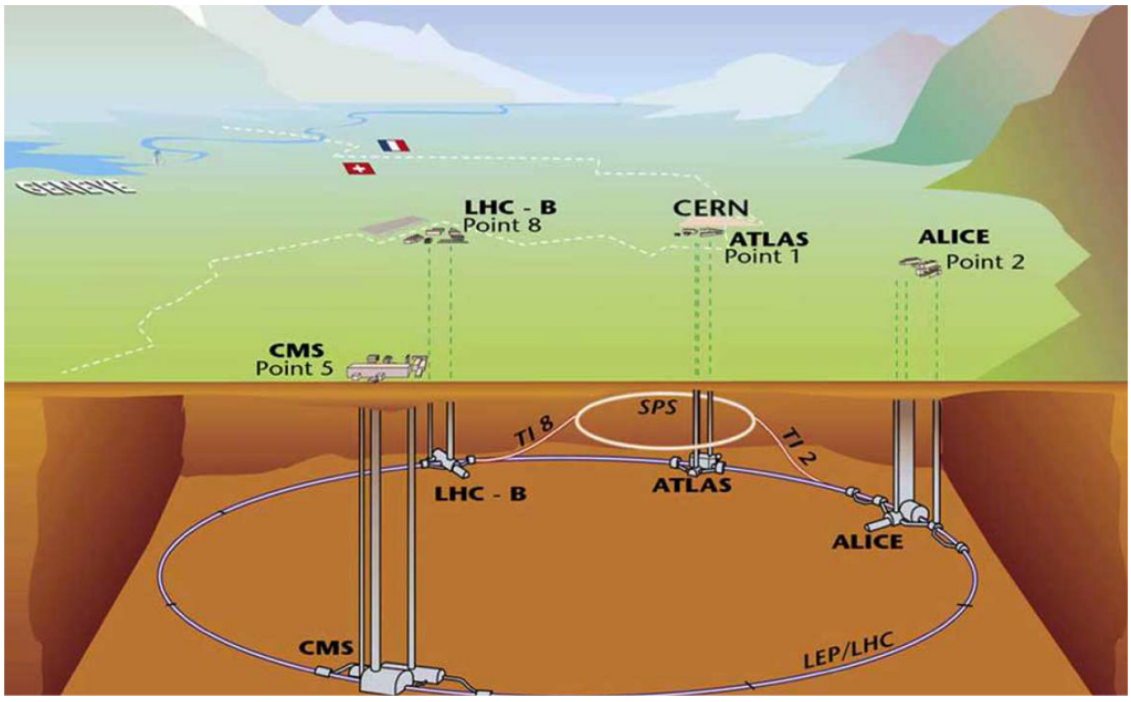

Figure 2.1: The Large Hadron Collider and CERN near Geneva, Switzerland [5]. Proton beams undergo a series of accelerations and transitions before reaching their final energy in the main ring and colliding with another beam traveling the opposite direction. The products of these collisions are then detected by several different detectors located at collision points.

The particle accelerator currently capable of reaching the highest energies is the Large Hadron Collider (LHC), shown in Fig. 2.1. It is located at CERN, the European Organization for Nuclear Research, on the border between France and Switzerland near Geneva. The LHC accelerates and collides bunches of protons. During the most recent LHC run, these collisions occurred at a center-of-mass energy

of 8 TeV, which is larger than the rest energy of a proton by a factor of approximately 10^4. Protons in these collisions are traveling 99.999997% of the speed of light by the time they reach the energy at which they collide. Eventually the LHC is expected to collide protons at an energy of 14 TeV, nearly ten times the largest energy achievable by any previous particle accelerator.

Collisions at the LHC occur at several different points along the main accelerator ring. The results of these collisions are observed and analyzed by the scientists collecting data from four different detectors along the ring: ALICE, ATLAS, LHCb, and CMS. Each detector collects data in a unique way, having a specific design based on the particular goals of its experiment. ATLAS and CMS are both general purpose detectors, intended to collect as much data from the collisions as possible, though each accomplishes this through different means. The CMS detector and its components are the focus of the research presented in this thesis.

2.2 The Compact Muon Solenoid (CMS) Detector

The Compact Muon Solenoid (CMS) is a general purpose detector designed to collect data from as many different collision-produced particles as possible. Its central feature is the powerful, high-quality solenoid magnet for which it is named. The magnet creates a magnetic field of nearly 4 Tesla in the interior of its cylinder. This causes the paths of charged particles to develop curvature as they scatter from collisions, allowing the experiment to gain valuable information about the momentum of the charged particles being observed. Outside of the solenoid are the muon chambers, the other component of the detector from which its name is derived. These contribute a great deal to the overall bulk of the detector, and they gather very important data on the muons scattering from collisions. These muons can be produced in abundance at the LHC, and they interact very little with the other detector components, making the muon chambers an essential part of data

collection. Several different cross-sectional views of the CMS detector are shown in Figs. 2.2–2.4.

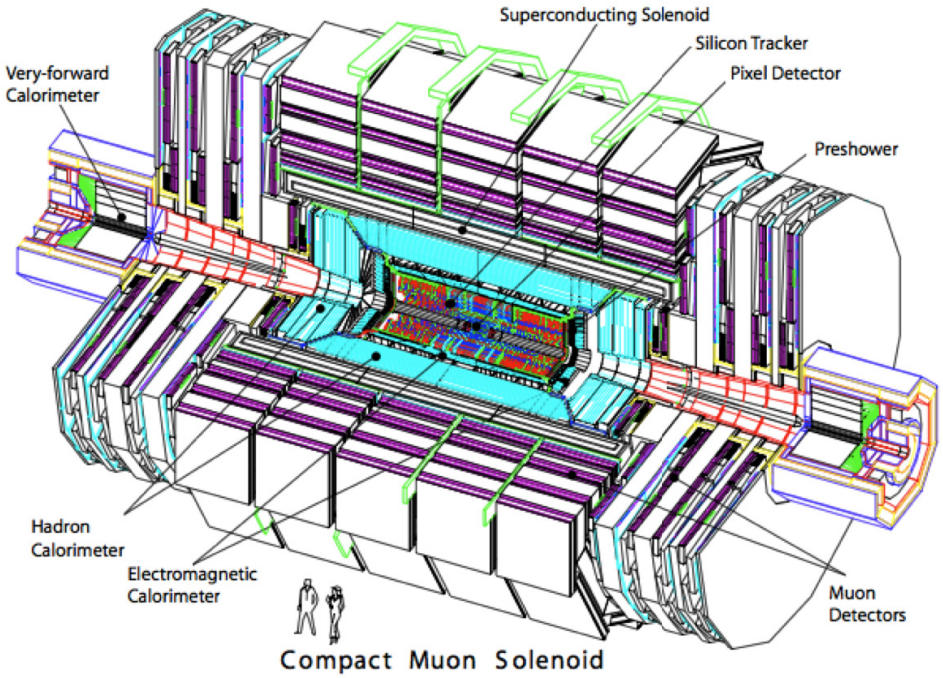

Figure 2.2: Cutaway view of the CMS detector showing the various layers and sub-detector components [6].

At the very center of CMS lies the beam line, the path along which high-energy protons enter the detector. The proton beams enter from both ends and collide at the center, scattering many types of particles in all directions. These scattered particles first encounter the silicon pixel tracker, which provides valuable information about the shapes and directions of particle paths in the detector. Outside the tracker is located the Electromagnetic Calorimeter (ECAL), which measures the energy of electromagnetically interacting particles such as photons and electrons. The next layer of CMS is the Hadron Calorimeter (HCAL), which is designed to detect hadrons, particles composed of quarks that interact through the strong force. Data from the

CMS detector are collected, stored, and then analyzed by the CMS Collaboration, a group composed of more than 3000 scientists from all over the planet.

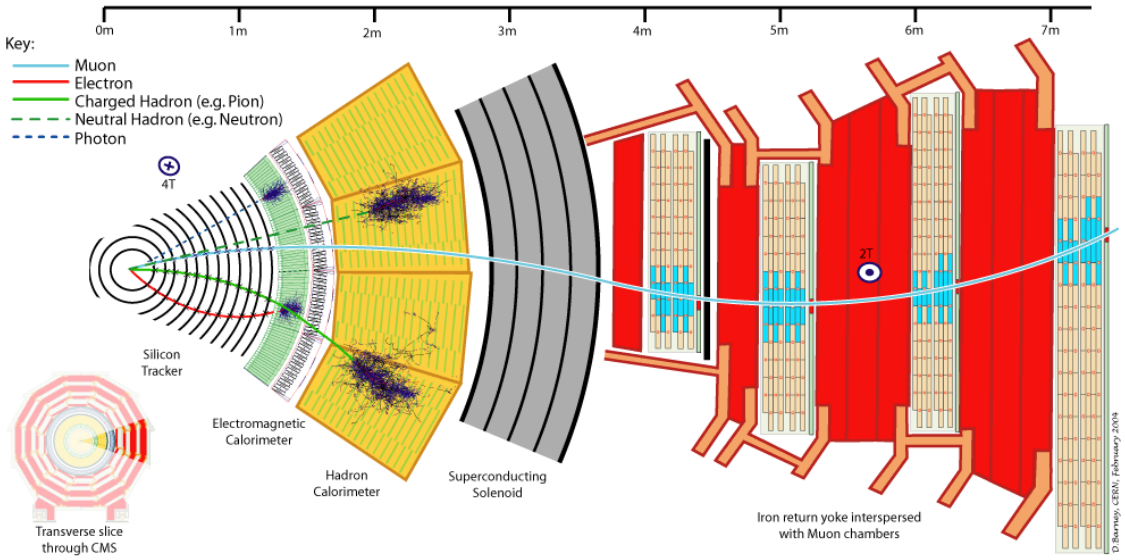

Figure 2.3: Transverse slice of the CMS detector with a wedge showing the main layers of detector components.

2.2.1 Hermeticity and Geometry of the CMS Detector

The high degree of hermeticity of the CMS detector is an important factor contributing to its success in detecting nearly all of the particles scattered from collisions at its center. Apart from the narrow beam line, the interaction point is almost completely surrounded by detector components in order to ensure that we have the opportunity to detect any particle that scatters away from the beam line at an appreciable angle. The nearly hermetic geometry of the detector assembly is what makes it possible to detect nearly all these particles, and this geometry can all be understood in terms of two variables which specify angles from the center: ϕ and η. CMS can be described by a right-handed coordinate system, with the origin at the center where collisions occur. The x-axis points radially inward with

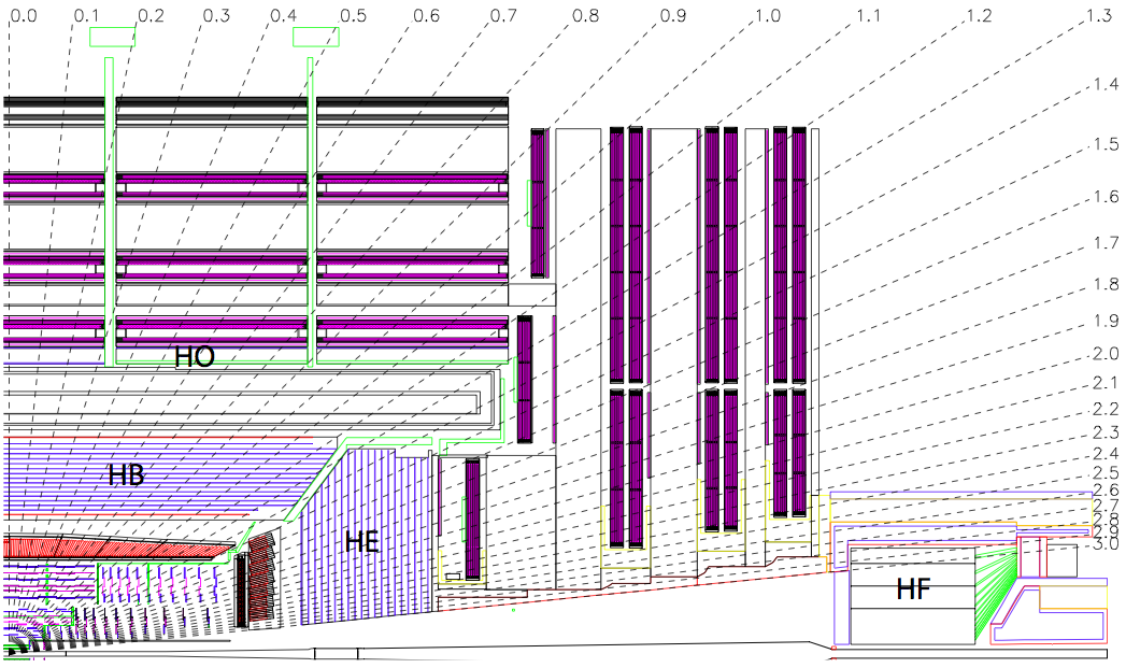

Figure 2.4: Upper right quadrant of a longitudinal cross section of the CMS detector, with the center of the detector in the bottom left corner of the picture. Four regions of the HCAL are labeled as the HB, HE, HF, and HO.

respect to the circle of the LHC, the y-axis points up with respect to the plane of the LHC, and the z-axis points along the counterclockwise beam direction. The polar angle θ is then measured from the positive z-axis, and the azimuthal angle ϕ is measured from the x-axis in the x-y plane [7]. Rather than θ, the variable more commonly used to describe the azimuthal angle is the pseudorapidity, which is defined as $\eta = -\ln[\tan(\theta/2)]$ [8]. Figure 2.4 shows a longitudinal cross section of CMS along with dashed lines representing various η values. The plane of Fig. 2.4 represents a constant ϕ value with varying η values.

2.2.2 The CMS Hadron Calorimeter (HCAL)

This thesis is primarily concerned with the HCAL component of the CMS detector, and this calls for a more detailed description of this particular subdetector. In the HCAL design, great attention is given to covering the largest possible values

of η possible, and this contributes greatly to the hermeticity of the detector. The HCAL consists of 3 major sets of components: the barrel (HB) covering $|\eta| < 1.3$, two endcap detectors (HE) covering $1.3 < |\eta| < 3.0$, and two forward calorimeters (HF) covering $2.8 < |\eta| < 5.0$, ensuring coverage of η from the center to very near the beam line. The HCAL also has a small layer outside of the CMS solenoid known as the HCAL outer barrel (HO), which is often associated with the HB for the purposes of our study since they cover the same η ranges. Figure 2.4 shows the locations of these four HCAL regions within the cross section of the CMS detector. The HCAL is segmented into different towers in η–ϕ so as to provide information on the location of hits detected within it, and these segments are assigned integer values of iϕ and iη. The iη segmentation is shown on the horizontal dimension of Fig. 2.6. A given set of one iη value and one iϕ value specifies a tower. In the HB for example, a tower extends radially outward from the beam line toward the solenoid, covering a range in η–ϕ space of $(\Delta\eta, \Delta\phi) = (0.087, 0.087)$. This segmentation scheme employs a total of 3600 towers to compose the entire HCAL.

The HCAL is a sampling calorimeter, composed of many interleaved layers of absorber materials and plastic scintillator tiles. The absorber material is brass in the barrel and endcap regions, and it is iron in the forward calorimeter region. Hadrons interact and produce many secondary particles as they pass through a plate of dense absorber material. These secondary particles can also interact with layers of absorbers as they encounter them, developing into a shower of hadronic particles (Fig. 2.5). As this shower progresses through the HCAL, it also encounters the scintillator materials, producing light signals. These optical signals travel to wavelength shifting fibers, which then carry the signals to readout boxes. Here the light signals are converted into electronic information for readout by photo-detectors (hybrid photodiodes in the present configuration). The amount of light collected by a photo-detector can be correlated with the total amount of energy of

the particles passing through the scintillators in the channel for which that photo-detector is responsible, and hence we gain valuable information on the energy of the incident particle that initiated the shower. In the present configuration, the iϕ and iη segmentation determines the regions to which photo-detectors are assigned, forming "towers" as all layers for a given iϕ and iη are read out into the same hybrid photodiode.

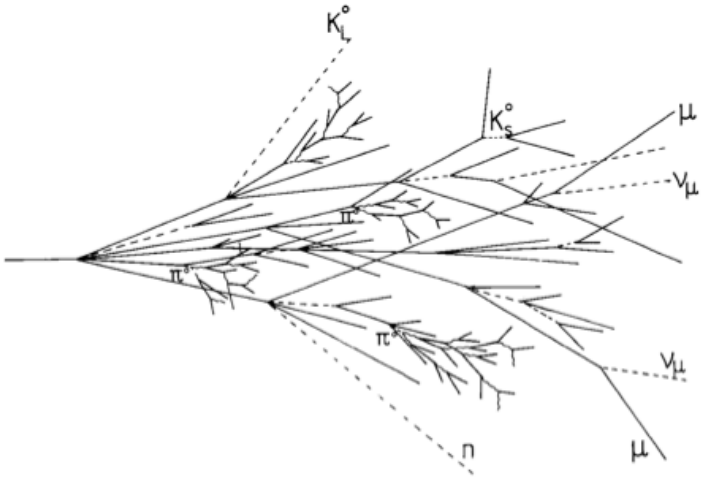

Figure 2.5: Example of a hadron shower in the CMS hadron calorimeter.

Hence, the HCAL collects information on the energies and positions of hadrons scattering from collisions, providing essential building blocks for event reconstruction. The HCAL data are also important for detecting hints of neutrinos or new, unknown particles, which can pass through the entire CMS detector unseen. Hadronic showers in the HCAL are important inputs for the global event description, also known as particle-flow (PF) event reconstruction [9], which reconstructs and identifies each particle visible to the CMS detector with an optimized combination of all subdetector information. All reconstructed particles are then used to calculate missing transverse energy, an essential variable for detecting particles that escape

CMS without depositing any direct signature. Missing transverse energy is calculated by examining the directions of energy signatures scattering from a collision, encoded in such measurables as hadronic showers in the HCAL. Conservation of momentum requires that these signatures be distributed in a balanced manner in the detector, unless a minimally interacting particle such as an neutrino carries away hidden energy. Supersymmetric candidate particles would also be likely to carry away energy in this manner, and thus missing transverse energy is an important variable for supersymmetry searches.

2.3 LHC Upgrade: Increased Energy and Luminosity

The LHC began colliding protons at a center-of-mass energy of 7 TeV in 2010. This operation continued through 2011, and after a short technical stop, it operated at a slightly higher energy of 8 TeV in 2012. The data collected during this time at these unprecedented energy scales enabled the discovery of the Higgs boson, but the LHC is still far from achieving its full potential for high-energy physics. In early 2013, the LHC shut down for a period anticipated to last almost two years, designated "long shutdown 1" (LS1). This shutdown allows opportunities for machine maintenance and upgrades. When the LHC begins running again after LS1, it will be able to achieve collisions with center-of-mass energy 13–14 TeV. It will run for several years at these energies before another one-year shutdown (LS2) scheduled in 2018. More LHC upgrades will occur during LS2, including upgrades that will enable it to provide higher luminosity to the detectors.

"Instantaneous luminosity" (or simply "luminosity") is a measurement of the number of particle interactions per unit time, essentially communicating the amount of data available to be collected by detectors such as CMS. "Integrated luminosity" refers to the time integral of luminosity, the total amount of data collected over a given time period. Typical units for integrated luminosity provided by the LHC

are $\text{fb}^{-1} = 10^{43}\ \text{m}^{-2}$. Currently, the LHC has provided approximately 30 fb^{-1} total integrated luminosity to its detectors. Between LS1 and LS2, the LHC is expected to provide an additional 200 fb^{-1} in the energy range 13–14 TeV. After LS2, the LHC will provide another 500 fb^{-1} at 14 TeV before a third long shutdown (LS3) scheduled to begin in 2022.

The entire period of time between initial 2010 runs and LS3 is designated Phase 1 of LHC operation. After LS3, the LHC is expected to enter Phase 2 of its operation, a ten-year high-luminosity period during which it is anticipated that it will provide an immense 3000 fb^{-1} of data. After Phase 2 is complete, the LHC may embark upon yet another upgrade project for Phase 3, with the goal of producing collisions in the energy range of 26–33 TeV. Phase 2 is sometimes known by the acronym "HL-LHC" (high-luminosity LHC), and Phase 3 by "HE-LHC" (high-energy LHC) as in Fig. 1.2.

2.3.1 Pile-Up

The LHC collides protons by accelerating two beams in opposite directions, such that they intersect near the very center of CMS and other detectors. Even with the extremely precise tuning of these beams, however, there is no guarantee that their intersection will lead to a collision that we will then be able to detect in CMS. Without these collisions, CMS would be left with very little interesting data. For this reason, the LHC collides groups of protons in bunches in order to increase the likelihood of producing head-on collisions when the beams intersect. Ideally, we would like to study the results of only one high-energy proton-proton collision at a time, but since the LHC collides protons in these large bunches, we in fact observe many proton-proton interactions within the same bunch crossing. This is not entirely unintentional, however, because these many interactions lead to much higher luminosity, and hence more data available for analysis.

This effect of many collisions occurring in a single bunch crossing is known as "pile-up," and it makes the analysis of particle collisions much more complicated. It is still possible to carefully sift through data to isolate and study individual proton-proton interactions, but this presents a serious challenge as the number of pile-up interactions increases. Bunch spacing, the time between the intersections of proton bunches within CMS, will decrease from 50 nanoseconds to 25 nanoseconds in the coming years in order to further increase luminosity. This decreased time interval further complicates the problems presented by high pile-up, since it increases the chances that the detector may still be registering hits from a previous collision even as the interactions from the next bunch crossing begin to unfold. The planned upgrades to the LHC will eventually increase pile-up to the point that there may be as many as 100–200 proton-proton interactions per bunch crossing (every 25 ns).

If we can find ways to overcome the challenges presented by high pile-up, however, the amount of data we gain is worth the effort. Particles such as Higgs bosons or supersymmetric candidates may only be produced very rarely even in high-energy collisions, so this increased pace of data collection enables us to approach their discovery much more rapidly. Increases in energy and luminosity at the LHC will create harsher operating conditions for detectors such as CMS, increasing the number of pile-up interactions and the amount of radiation to which the detector must be resilient. This will present challenges for continued data collection and interpretation as well as detector upkeep, but the overall advantages for potential physics discoveries make these increases worthwhile.

2.4 CMS Hadron Calorimeter Upgrade

In order to deal with the increased energy and luminosity at the LHC, the CMS detector will undergo a number of upgrades over the coming years. These will enable the detector to continue to collect high-quality data even as conditions at the

LHC become increasingly harsh. The HCAL is a major part of the planned Phase 1 upgrades to CMS during LS2, and this section provides a brief outline of the major aspects of the planned HCAL upgrade. More details can be found in Ref. [10].

2.4.1 Silicon PhotoMultipliers and Multi-Anode PMT's

Improved photomultipliers will replace the old hybrid photodiodes (HPD's) currently used for HCAL readout. In the HB and HE, these HPD's will be replaced by Silicon PhotoMultipliers (SiPM's), which are more reliable and much smaller, occupying an area of only a few mm^2. Using smaller photomultipliers makes it possible to fit many more of them within the compact spatial confines available for readout electronics in CMS. These SiPM's also have much higher gain than the old HPD's, making them generally a higher quality photo-detector, with better sensitivity to lower energies that may be collected from a small HCAL region. The increased number of photo-detectors with higher gain will make it possible to create many more readout channels, leading to finer segmentation for HCAL data readout. In the HF, multi-anode PMT's will be installed. More on the technical advantages of these instruments can be found in the technical proposal for the upgrade of CMS [10].

2.4.2 Depth Segmentation

The segmentation in the angular directions was discussed in Section 2.2.2, but what about the radial direction? The HCAL has many different scintillator layers in the radial direction (17 in the HB and 18 in the HE), but the present version of the detector reads all of these layers out into a single channel, so some information about the hadron shower development within the HCAL in the radial direction is lost. The SiPM's to be installed will make many more channels available for readout. The upgraded HCAL will segment the radial direction into several different depths, with the scheme depending on the region of the HCAL, shown in Fig. 2.6. The

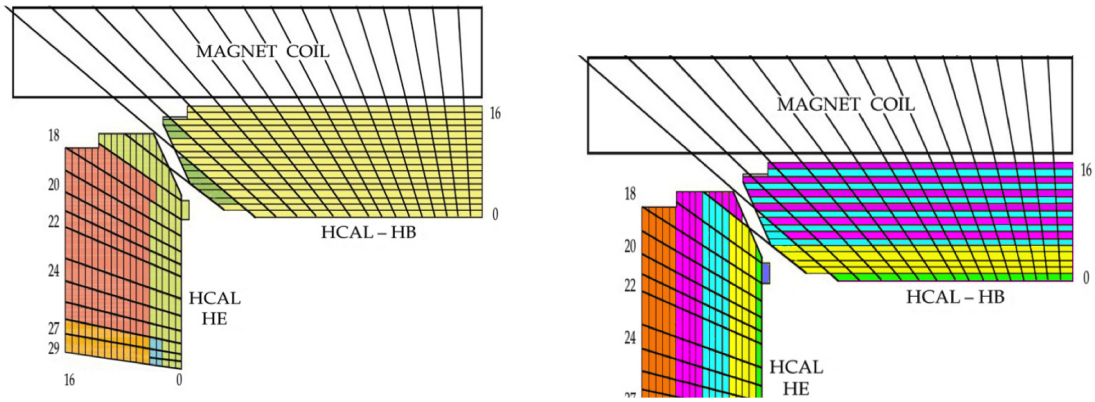

Figure 2.6: Current HCAL segmentation scheme (left) and upgrade segmentation scheme (right). The horizontal direction represents iη segmentation, while vertical represents depth segmentation (radial direction for the CMS cylinder). Color blocks represent the channels into which the scintillator layers are grouped for readout.

alternating depth segmentation scheme for the outer depths of the HB introduces a redundancy in the later depths to safeguard against channel failures. This depth segmentation will allow us to gain greater resolution in the data for how deep within the HCAL interactions are occurring, yielding more information about the geometry of hadron shower development in the HCAL.

2.4.3 Charge Integrator and Encoder (QIE) and Time to Digital Converter (TDC)

The final major category of upgrades to the Hadron Calorimeter involves the electronics used to read out and record the data being collected. These electronics collect the analog electronic information sent from the photo-detectors and convert it into the digital form that will ultimately be stored and used for analysis. This is accomplished by a chip called the Charge (Q) Integrator and Encoder (QIE). The old, version 8 chips (QIE8) will be replaced by upgraded, version 10 chips (QIE10) [11]. This new version incorporates Time-to-Digital Converter (TDC) timing information along with its Analog-to-Digital Converter (ADC) digital output, and it will be tuned specifically to complement the SiPM characteristics. The ADC converts analog

charge pulse signals being collected from the photomultiplier into digital units, which are easy to store, access, and relate to the energy being deposited in the detector. The TDC collects time information associated with these hits by recording a digital value when the energy pulse in its channel has passed a certain threshold. The TDC also records another value associated with the same pulse when it falls below the specified energy threshold.

A graphical representation of pulses from hits in the HCAL and the timing values recorded by the TDC is given in Fig. 2.7. Notice that the higher energy pulse will cause the TDC to record a time value near 2 ns, while the lower energy pulse takes longer to pass the threshold and will record a time value near 3 ns, despite the fact that both pulses take place at essentially the same time in reality. When this TDC timing information is properly calibrated and corrected, we gain roughly 1 ns resolution on the timing of hits in the HCAL. Having access to this high-resolution time information will provide great advantages for accurate collision reconstruction by allowing for background rejection and other corrections. This TDC calibration process and the background rejection it enables are the topics of subsequent chapters.

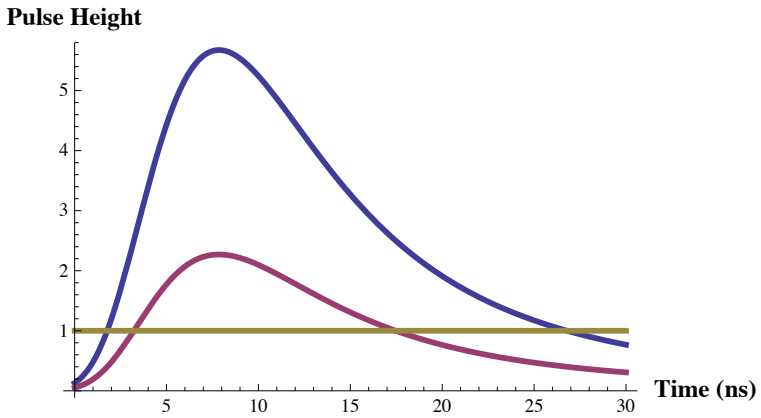

Figure 2.7: Energy pulses passing the TDC threshold. The TDC will record a digital value representing the time when the pulse energy passes the threshold, as well as a "time falling" value associated with the same pulse when it falls back below the threshold.

CHAPTER THREE

Simulation and Calibration of TDC-Based Time

In general, upgraded components and improved electronics will certainly provide advantages for particle detection in CMS, but we wish to gain a more detailed picture of the form these advantages will take. The specific setting of the CMS detector configuration will present a unique set of circumstances for the operation of these upgrade components. We desire to gain a detailed understanding of their behavior in this setting before their installation in order to know exactly what to expect. We can then optimize their usage accordingly. This knowledge is also essential for gaining final project approval for the upgrade, since the total cost of the proposed HCAL upgrade will be around eight million CHF, and we need sufficient physics-based motivation to justify such an expense. Since the actual physical configuration of CMS is currently inaccessible, we must turn to highly involved simulations to accomplish this goal of understanding the upgraded components in their proposed configuration as a part of CMS.

3.1 Validating and Refining Simulation Releases

Fortunately, detailed simulations have long played a significant role in the work done at CMS, and hence highly developed simulation tools exist for investigating particle interactions in CMS according to well understood and important physics processes. These tools provided a robust structure upon which the simulations of an upgraded CMS detector could be built. Once the specific components and their configuration within the CMS upgrade were determined, simulations of particle interactions in the upgraded detector were developed over the course of 2011 and 2012. These simulations took the form of a series of software releases within the larger CMS computing framework, each building upon and refining the developments

of the last. The following software releases within the CMSSW framework were used at various stages of our study.

- `CMSSW_4_2_8_SLHChcal`
- `CMSSW_4_2_8_SLHChcal2`
- `CMSSW_4_2_8_SLHChcal2_patch2`
- `CMSSW_4_2_8_SLHChcal3`
- `CMSSW_4_2_8_SLHChcal4`
- `CMSSW_4_2_8_SLHChcal4_patch3`
- `CMSSW_4_2_8_SLHChcal4_patch4`
- `CMSSW_4_2_8_SLHChcal5`

These software releases provided the ability to simulate a wide array of particle interactions occurring within a CMS detector with the very specific materials and geometry of the upgraded HCAL and silicon pixel tracker, another significant aspect of the planned CMS upgrade. One of our primary tasks during the initial stages of the research conducted for this thesis was examining various aspects of these simulation releases and validating them for appropriate usage in our studies.

3.1.1 Periodic Structure Revealed by TDC Simulation

A brief examination of the periodicity of groups of hits in the HCAL verses the ECAL will provide a representative example of the work that was involved in validating the simulation releases. The simulation releases that we used were designed by modifying the simulated structure of the HCAL and its readout electronics in accordance with the planned upgrades, while building the rest of the simulation on the basis of existing tools that were already well-validated and ready for use. In this particular case, we were able to use timing information being collected by the ECAL in the simulations to identify and correct problems with early versions of the simulation for the upgraded HCAL.

Until 2012, the LHC collided proton bunches every 50 nanoseconds, so we had a great deal of experience simulating these conditions. The upgrade simulation releases were intended to reflect the operating conditions for the upgraded CMS detector, and hence the spacing between bunch crossings should be 25 ns, as discussed in Section 2.3.1. This spacing should lead to a periodic structure of the time data collected in the detector, with a period of 25 ns between peaks in energy pulses. As we began to investigate pile-up, we saw exactly this periodic structure reflected in the energy collected by the ECAL (Fig. 3.1). So the relevant code for ECAL reconstruction was handling this change without any problems, but it turned out that the first attempts at HCAL aspects of these simulations did not run quite as smoothly. In early releases (`CMSSW_4_2_8_SLHChcal4_patch3` and before), the periodicity of hit times being recorded by TDC's in the HCAL was 50 ns rather than the 25 ns that it should have been.

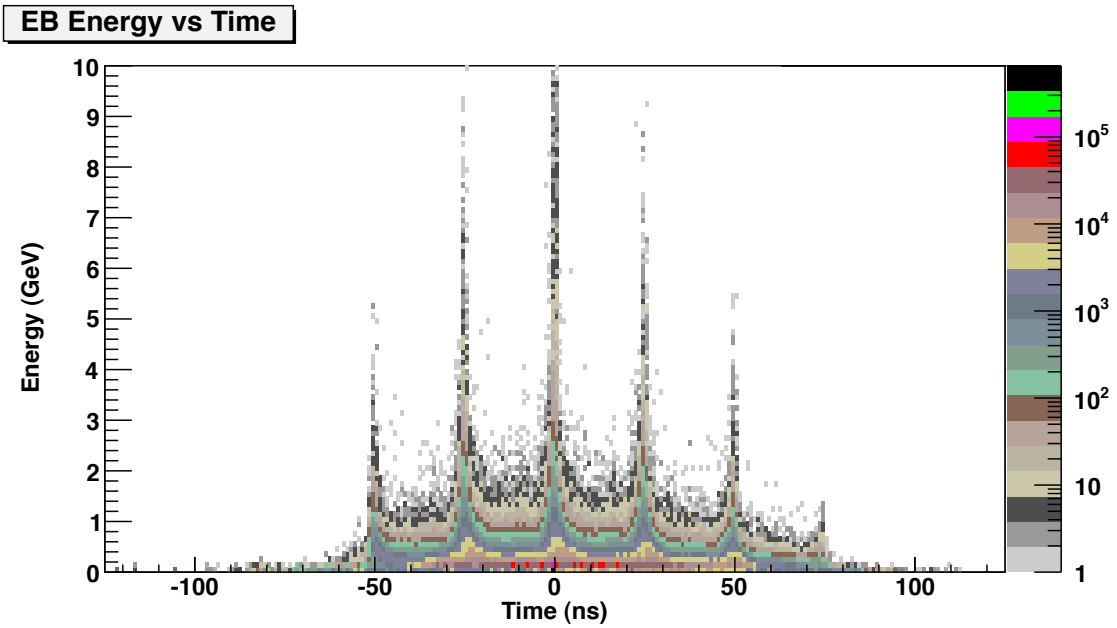

Figure 3.1: Energy vs. time for hits in the barrel of the electromagnetic calorimeter from a simulated sample including pile-up (from release `CMSSW_4_2_8_SLHChcal4_patch3`). The 25 ns spacing between peaks is exactly what was expected.

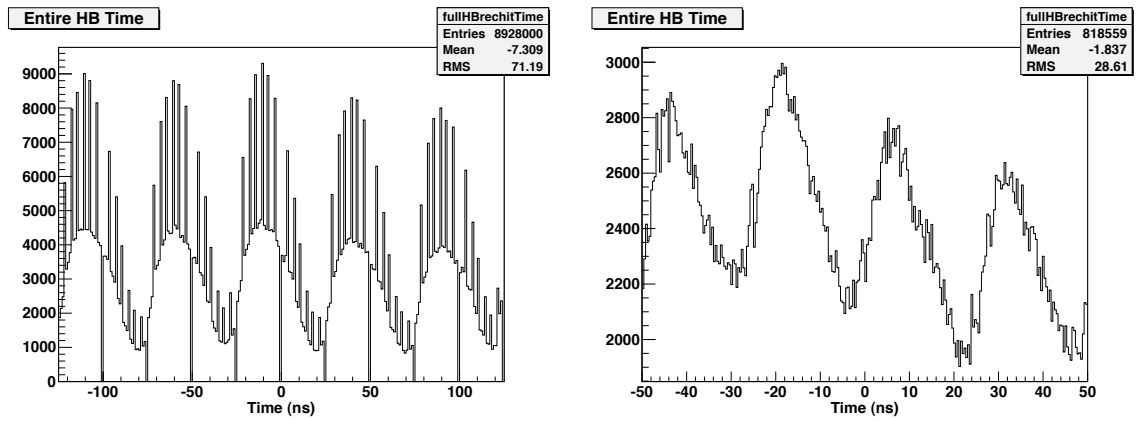

Figure 3.2: Time distributions of hits over the entire HCAL barrel from an older simulation release (`CMSSW_4_2_8_SLHChcal4_patch3`, left) and a newer release after the bug fix (`CMSSW_4_2_8_SLHChcal5`, right). Note that the time between peaks decreases from 50 ns to the 25 ns that was expected. Note also the elimination of the gaps every 25 ns that appear in the older time distribution. These blind spots were eliminated due to a refinement of the encoding for TDC digital values.

Once this problem was identified, we were able to notify those responsible for the development of these simulation releases and aid in the process of fixing the bug. Simulations involving pile-up done in subsequent releases revealed proper periodic structure of hits in both the ECAL and the HCAL (see the right of Fig. 3.2). Many other checks of this nature were performed, though of course very few brought to light problems of this scale, and in general modifications and fine-tuning (such as the refining of the TDC encoding to eliminate small blind spots) were somewhat easier to implement.

3.2 Calibrating Time Information Collected from the TDC

As the simulation releases for the upgraded HCAL became more refined, we began to encounter the benefits of detailed simulation at this level, and this was nowhere more evident than in the understanding that we gained from this study on how the TDC will record and encode time values. This understanding provided the

ability to calibrate the TDC-based time information that will be gathered from the detector, and this greatly improved the resolution of timing information collected. Referring back to Fig. 2.7, one will notice that the time value recorded for a lower energy pulse will be somewhat later, since it takes longer to pass the TDC threshold, despite the fact that it occurs at essentially the same time as the higher energy pulse in reality. Our simulations revealed that there is indeed a strong correlation between the energy of a hit in the HCAL and the time value the TDC records for that hit.

Once the correlation between hit energy and TDC-based time was observed, we were able to fit the profile of the curve observed in the time vs. energy plane to a function of the form $t = a + b/(c + E)$, where t is time, E is energy, and the other constants are fit parameters. We performed these fits for three different depths of the HCAL barrel, since timing of hits varies slightly as particles arrive later in successive depths. Figure 3.3 displays the fits for all three depths. With these fit functions in hand, we were able to adjust the "late" time values recorded at lower energies toward the asymptotic value of the fit function, which represents the real time at which the pulse began (essentially the same as the TDC-recorded value for very high-energy hits). This calibration of the TDC-based time values for low-energy hits improves the time resolution to nearly 1 ns. The significant advantages provided by this increased resolution will become evident in the corrected time distributions for beam halo particles discussed in the next chapter.

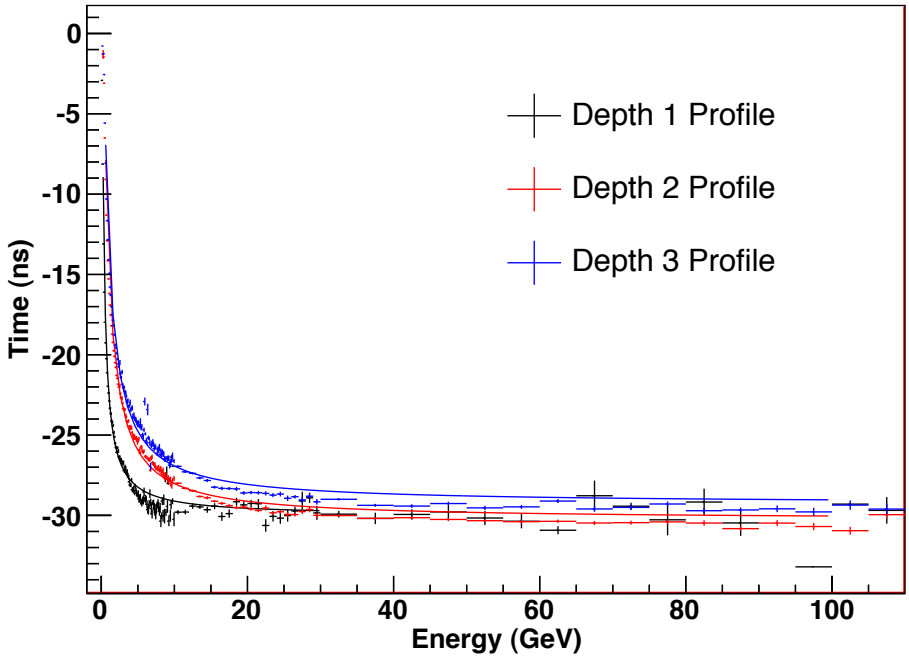

Figure 3.3: Time vs. energy fits for hits in the HCAL barrel. Fits are done separately for each of the 3 different depths in the HB, since hits arrive slightly later in successive depths.

CHAPTER FOUR

Non-Collision Background Rejection Using the TDC

All experiments face the challenge of distinguishing backgrounds from desired data, and CMS is no exception. Ideally, backgrounds can be minimized or eliminated by some method such as shielding the apparatus. The CMS detector, for example, is located far underground in order to minimize the background of energy deposited in the detector by cosmic rays. It is not always possible to eliminate all backgrounds simply by shielding the apparatus though, and this necessitates finding methods of recognizing and rejecting backgrounds in the data after collection. The CMS detector encounters one such unavoidable background in the form of stray particles from the LHC known as beam halo particles, which approach the detector from just outside the beam line. This chapter examines the advantages provided by TDC-based timing information in recognizing and rejecting this significant background.

4.1 Beam Halo

The massive, circular accelerator at the LHC produces beams of protons with energies on the scale of 3.5–7 TeV. Objectively, the energy of a proton at 7 TeV $\approx 10^{-6}$ J is not enormous, until one considers the minute size of the object endowed with that amount of energy. Protons with energies on the TeV scale travel at relativistic speed, emitting large amounts of energy in forms such as synchrotron radiation, so a great deal of effort and precision is required to force the protons at the LHC to attain such high energies. The complexity of the apparatus used to produce these protons suggests that this process is neither simple nor perfectly precise. Artifacts of the imperfect production of these high-energy proton beams at the LHC arise in such forms as beam halo particles, the background with which this study is concerned.

As protons are accelerated around the circle of the LHC, the beam develops a "halo" of particles around it traveling parallel to the beam line, and some of these particles eventually hit the CMS detector. Particles from the beam halo that hit the CMS detector are primarily muons, and when a muon traveling in this halo acquires sufficient energy, it can radiate and leave a substantial energy signature in the HCAL. Depositing unpredictable energies that are not related to the collisions we wish to study, these beam halo interactions in the detector present a serious challenge to accurate reconstruction of the collisions occurring at the same time. Beam halo is a well documented background that CMS has been dealing with for years, and methods already exist for mitigating the problems of contamination by beam halo interactions. These methods, however, are often rather involved and imperfect at identifying and removing contamination [7]. Upgrades to the CMS detector, on the other hand, could provide more elegant, straightforward, and powerful solutions for discarding beam halo deposits while keeping interesting signal from collision-related hits.

The halo formed around the proton beams can be large enough for beam halo particles to pass directly through the CMS HCAL, up to three meters away from the beam line. Study of beam halo is therefore an important part of the HCAL upgrade. In particular, we wish to investigate the advantages provided by TDC-based timing for dealing with beam halo contamination of hits in the HCAL. As before with our TDC study, we proceeded by means of the detailed simulation tools for the upgraded HCAL that were available, refining them where necessary. Tools for the simulation of beam halo production were also available. Thus, once the simulation of the upgraded detector and our understanding of its TDC-based timing reached a sufficient level of maturity, we were able to combine the simulation tools to reproduce an accurate representation of beam halo interactions in the upgraded CMS HCAL. We first simulated beam halo interactions with the upgraded HCAL

in isolation, and later we compared these to the timing and energy information we had gathered from simulations of collision-produced particles in the detector.

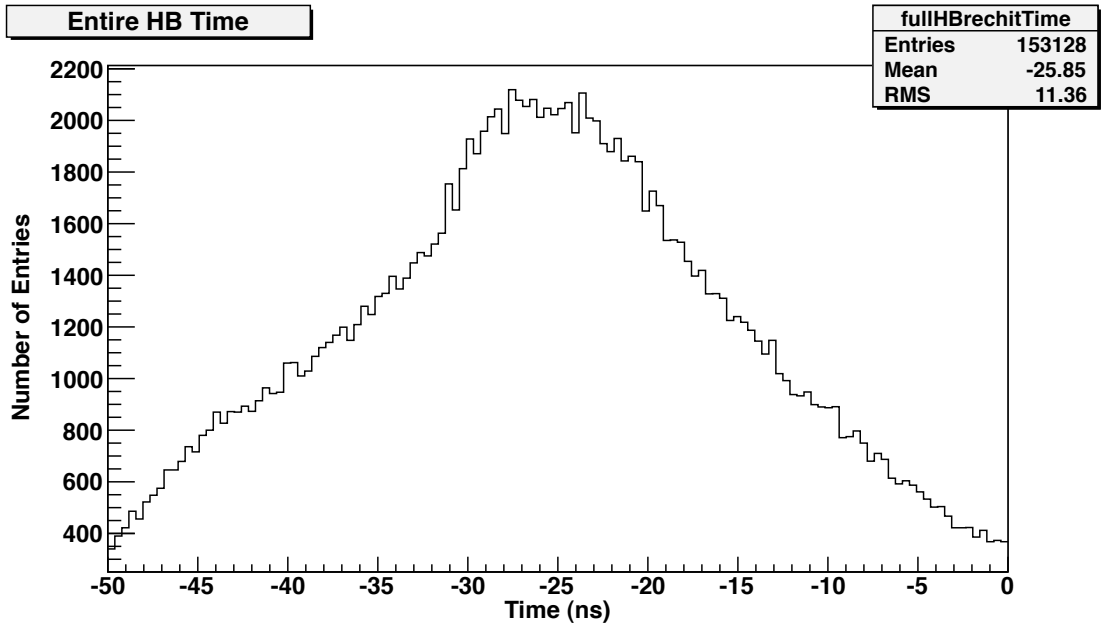

Figure 4.1: Beam halo time distribution for the entire HCAL barrel (HB). Notice how many entries are distributed over a wide range of time values, varying from –50 ns (well before the signal from collisions would arrive) to 0 ns (well after the signal has deposited most of its energy in the HCAL).

An initial look at the time distribution of beam halo hits in the HCAL reveals very little. The time distribution is very wide, with timing of beam halo hits spread from well before the collision occurs to well within the time window of hits caused by the particles scattered from the collision (Fig. 4.1). This is where the TDC time correction discussed in the previous chapter becomes an important factor in recognizing the differences between beam halo hits and signal hits. The other essential factor in recognizing these differences is understanding the geometry of the paths of beam halo particles through the HCAL. Once this geometry is well understood, it

is easy to take advantage of the iη segmentation of the CMS HCAL in conjunction with the corrected TDC time to recognize the patterns left by beam halo hits.

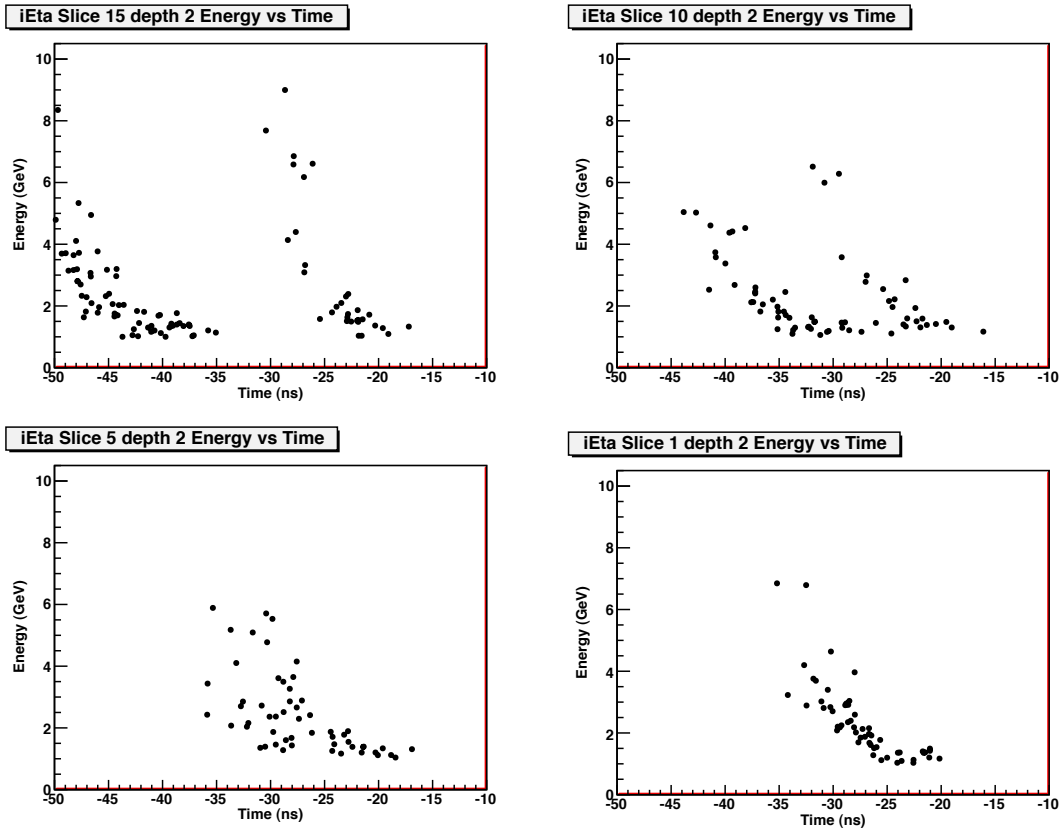

Figure 4.2: Patterns of beam halo hits in energy vs. time plane at various iη slices in the HCAL barrel. Notice the two distinct groups, corresponding to the beam halo particles arriving from both sides of the detector. The earlier group arrives from the near side of the detector, and the later group comes from the far side. These two groups overlap near the center of the HCAL at i$\eta = 1$. Notice also the distinctive curvature of the groups of hits. Once this is corrected using the fits described in the previous chapter, we can obtain very narrow distributions of beam halo times for a given iη slice.

Beam halo particles enter the CMS detector from both ends and traverse it parallel to the beam line. Particles on the GeV and TeV energy scales of the LHC travel very close to the speed of light, but the nanosecond resolution of the TDC should enable us to see the finite amount of time it takes these particles to travel

distances on the scale of a few meters. The simulations reveal that beam halo hits leave distinct patterns in the TDC times with energies deposited at slightly different times depending on how far into the detector they have traveled. This time dependence is most easily discerned looking at the iη dependence of beam halo times in the HCAL barrel, as displayed in Fig. 4.2. When plotted in the energy vs. time plane, we see clear patterns of hits for each iη slice, and these suggest the usefulness of the TDC time correction in resolving beam halo times. The HCAL endcap is oriented perpendicular to the barrel, so in the case of the endcap the depth segmentation can be used to see a similar pattern.

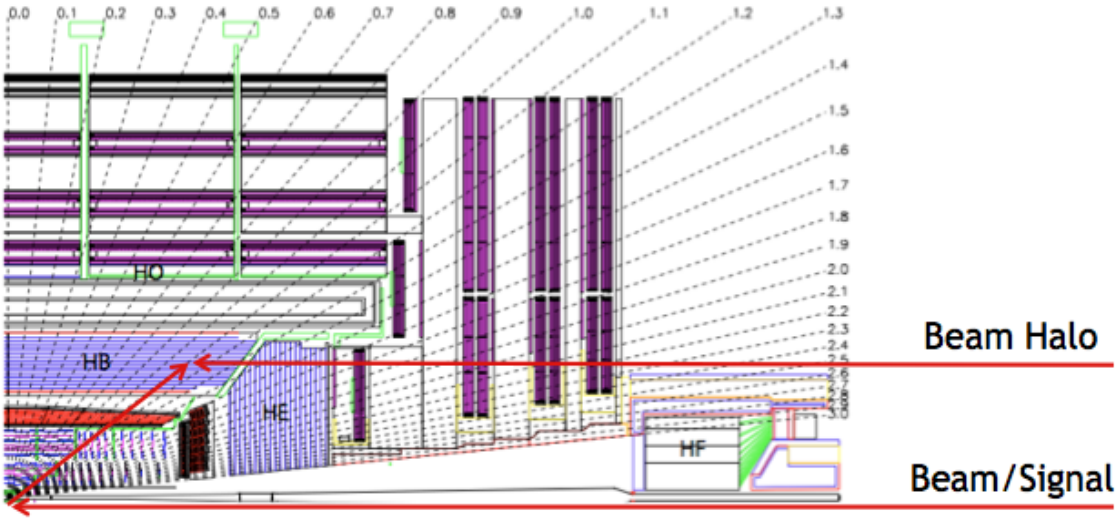

Figure 4.3: Longitudinal cross section of CMS showing paths of beam halo and collision-produced particles to the HCAL. Beam halo particles travel parallel to but outside of the beam line. Their paths to the HCAL are more direct and several meters shorter than the paths of particles scattering from collisions at the center of CMS, so beam halo particles arrive a few nanoseconds earlier.

Once we recognize these hit patterns for the different iη slices of the HCAL barrel, it is straightforward to apply the TDC time correction described in the previous chapter. This will provide us with a reasonably narrow time distribution for

a given iη slice, and we can then compare this distribution to that of the other hits arriving along with the beam halo particles. Since the beam halo particles take a more direct path to the HCAL (see Fig. 4.3), they arrive a few nanoseconds earlier than signal from collisions. So once we have achieved sufficiently narrow time distributions for both groups of hits, we should be able to use the TDC-based time to reject a great deal of beam halo background.

4.1.1 Central Regions of the HCAL

Near the center of the detector, beam halo particles from both sides of the detector arrive at the same time, forming one large group of hits. We compared the time distribution of these hits to that of pions representing signal scattered from collisions at the center of the detector. Once we corrected both distributions based on the TDC time fits, we obtained the striking comparison displayed in Fig. 4.4 for the very center of the detector at i$\eta = 1$. Beam halo hits arrive five to ten nanoseconds earlier than the pions, just as we would expect based on the path length difference of a few meters. With corrected TDC time distributions this narrow at this resolution, applying a cut at a value near -34 ns would cut out nearly all of the beam halo contamination while preserving the interesting pion signal. This demonstrates the power of the TDC in providing simple, elegant solutions for background rejection that were not previously available. Once properly calibrated, the TDC-based time is sensitive to differences of a few nanoseconds, providing a powerful time measurement tool for the HCAL.

4.1.2 Outer Regions of the HCAL

In outer regions of the HCAL, the situation is not quite as neat as what we found in the center. In this section, we examine the i$\eta = 10$ slice as representative of the situation near the periphery of the HCAL barrel. Here the beam halo particles

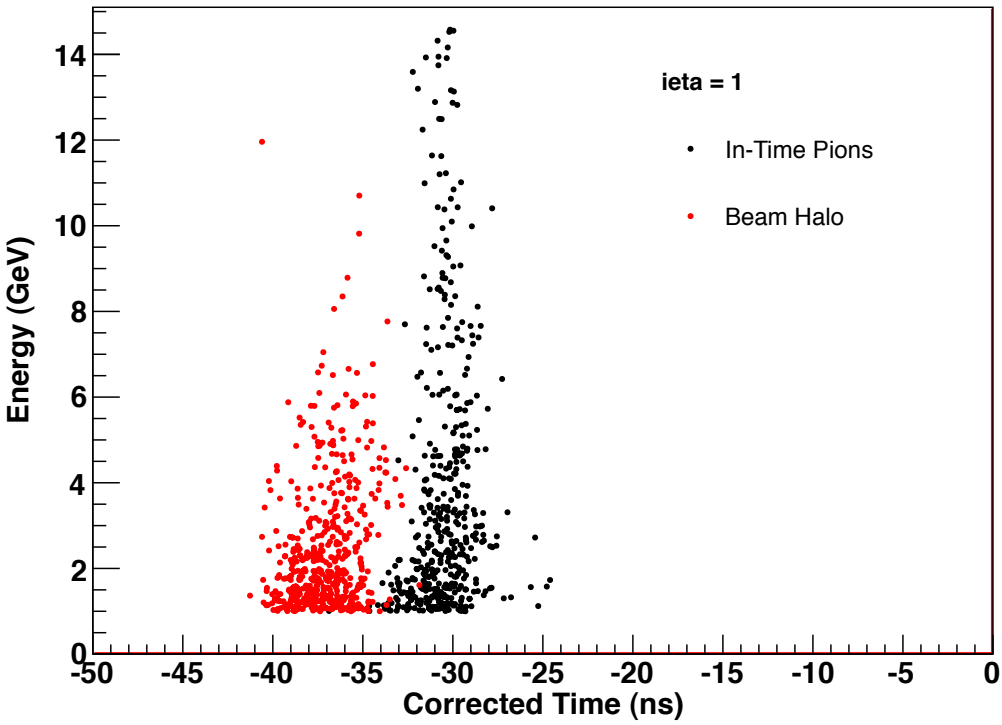

Figure 4.4: Energy vs. time histogram showing both in-time pion signal and beam halo hits at i$\eta = 1$ (center of the HCAL).

form two distinct groups of hits (Fig. 4.5), since one edge of the detector is much closer than the other to this slice of the HCAL. The group of beam halo particles arriving from the near side of the detector records corrected TDC time values much earlier than the pion signal, and it is easily rejected. The group arriving from the far end, however, travels much farther before interacting with this portion of the detector. This group barely arrives before the signal from the collision, and we observe some overlap between the beam halo and signal hits. Cutting based on TDC time alone will enable us to reject more than half the beam halo contamination in this case, but it does not provide the power to remove the hits overlapping with the signal. So we see that there are limitations to our ability to remove all beam halo background based on TDC time alone, and other considerations such as the

topology of beam halo hit patterns may be necessary to remove the remainder of the beam halo contamination.

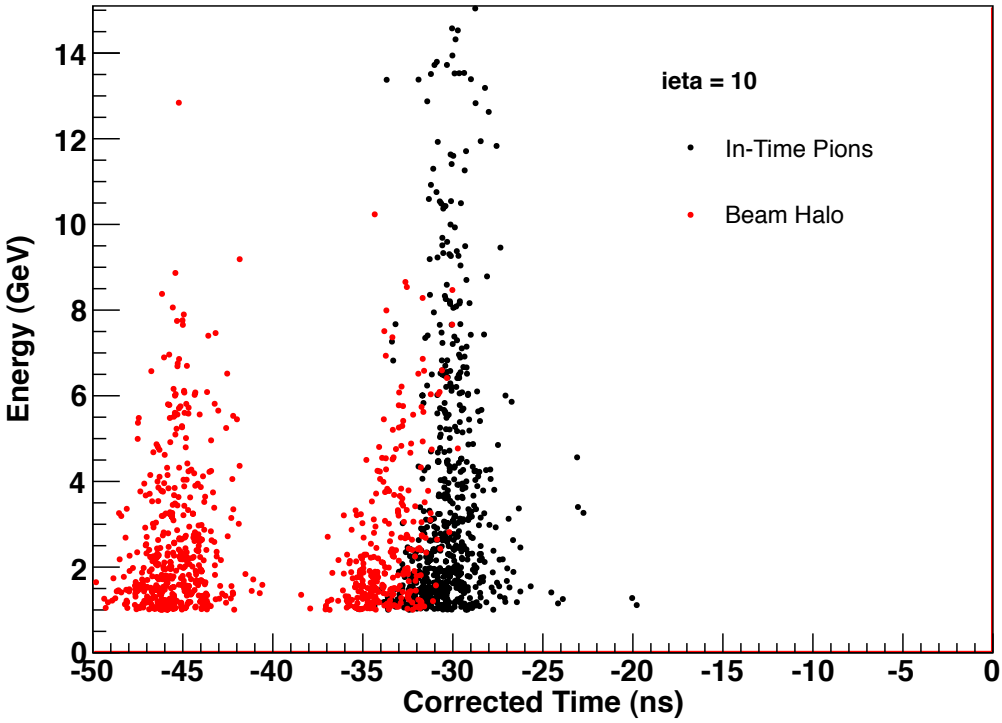

Figure 4.5: Energy vs. time histogram showing both in-time pion signal and beam halo hits at $i\eta = 10$ (outer region of the HCAL barrel).

CHAPTER FIVE

Conclusion

The LHC was constructed in order to study fundamental particle physics in an energy regime not achievable by any previous accelerator. It has already accomplished one of its major goals in the discovery of the Higgs boson, but many more exciting discoveries and measurements lie potentially within reach of the LHC. For this reason, the LHC will be upgraded to increase energy and luminosity provided to detectors such as CMS. In order to cope with this increasing energy and luminosity provided by the LHC and take full advantage of the data available to it, the CMS detector will be upgraded in the coming years. As part of this upgrade, new electronics will be installed in the hadron calorimeter, including Silicon PhotoMultipliers and new Time-to-Digital Converters. Not only will these upgrades help mitigate the increased strain on the detector (from sources such as increased pile-up and decreased bunch spacing), they will also provide advantages for particle reconstruction that are not available in the current CMS configuration.

Simulation studies of TDC-based time information revealed a definite correspondence between hit energy and time recorded. We were able to perform fits of the time vs. energy profiles for various regions of the detector, and subsequent calibration of TDC-based time values improved resolution of hit timing information to nearly 1 ns. This resolution proved especially useful in rejecting unwanted backgrounds such as hits from beam halo particles, which often arrive in the detector a few nanoseconds earlier than the hits resulting from proton-proton collisions. Simulations of beam halo samples revealed that properly calibrated TDC-based time possesses sufficient resolution to distinguish the majority of beam halo hits from collision interactions, though results do vary somewhat depending on the geometri-

cal region within the HCAL. This makes it possible to reject a great deal of beam halo background based on the TDC timing information alone, and this provides improvements over the current beam halo identification and rejection scheme, which primarily uses the forward muon detectors [7].

This ability to reliably reject important backgrounds like beam halo hits demonstrates the power of the TDC aspect of the CMS HCAL upgrade. Background rejection at this level will have far-reaching positive effects on event reconstruction at CMS, strengthening our ability to obtain key analysis information from variables such as jets and missing transverse energy [9]. At this stage, we are only beginning to understand the full power of TDC-based time information, and it is anticipated that this timing will also be extremely beneficial in avoiding the problems caused by high pile-up and decreased bunch spacing. These significant advantages provided by the TDC functionality of an upgraded CMS detector will ultimately improve our ability to make new discoveries and breakthroughs in physics as the LHC continues to run and CMS collects more data, and this possibility provides strong motivation for the carrying out the intended upgrades. The studies presented herein on TDC calibration and beam halo rejection formed a portion of the HCAL technical design report [11], which helped procure final approval for the proposed CMS HCAL upgrades.

APPENDIX

APPENDIX A

CL_s Statistical Methods and Supersymmetry Exclusion

The Constrained Minimal Supersymmetric Standard Model (CMSSM) is especially interesting from an experimental standpoint because it lends itself to description and experimental probing in terms of just two key parameters: the common gaugino mass ($m_{1/2}$) and the common scalar mass (m_0). It is "minimal" in the sense that it contains only a minimal number of supersymmetric particles necessary to make theory consistent with current data. It is "constrained" in such a way that the many possible parameters of supersymmetry can be related back to the key $m_{1/2}$ and m_0 parameters for this particular formulation.

The two key CMSSM parameters derive their names from the fact that they are the two values to which supersymmetric particle masses will converge at some unification energy scale. The common gaugino mass ($m_{1/2}$) is the value at which the various gaugino masses unify for energy at the unification scale. The common scalar mass (m_0) is the value at which the squark and slepton masses will unify on this same scale. Figure A.1 shows the characteristic evolution of supersymmetric particle masses toward this unification scale for $m_0 \approx 200$ GeV/c^2 and $m_{1/2} \approx 600$ GeV/c^2 with unification occurring at an energy of 2×10^{16} GeV. The two key $m_{1/2}$ and m_0 parameters are not yet known, however, so we must find their values through experiments. The figure only shows what CMSSM might look like with certain specific values for $m_{1/2}$ and m_0, and in fact those particular values have already been excluded according to Fig. 1.1.

If signs of CMSSM were to present themselves in the CMS data, theory predicts that they will leave signatures in the form of missing energy and momentum. Standard model processes also leave signatures of this same form, due to sources such

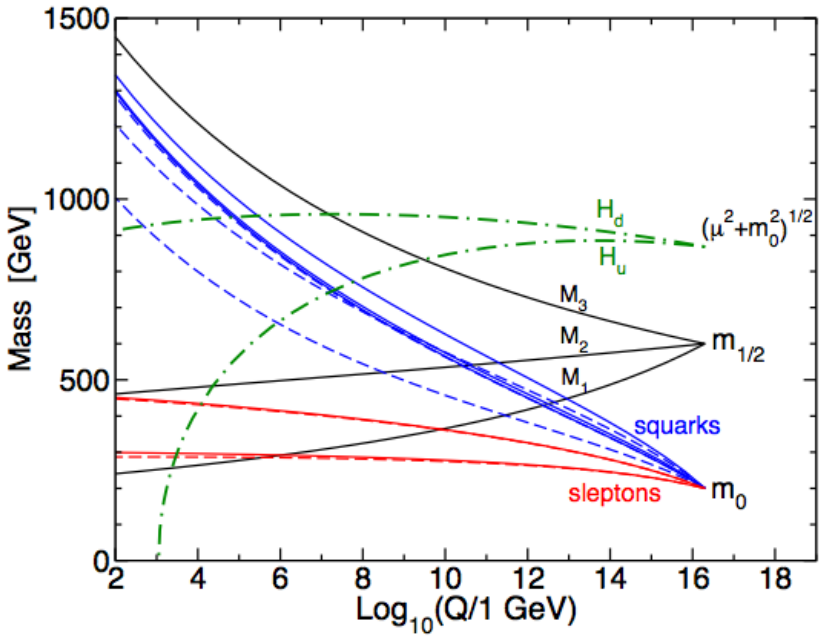

Figure A.1: Evolution of supersymmetry particle masses toward $m_{1/2}$ and m_0 parameters at the unification scale according to CMSSM [12].

as neutrinos carrying off energy from collisions without interacting with the CMS detector. These standard model processes form significant backgrounds, so the task becomes discerning supersymmetry signatures from standard model backgrounds. Detailed studies based on the collision data and Monte Carlo simulations provide predictions for production rates of missing energy and momentum due to well understood standard model processes. If one can then discern an excess of events with these signatures in the data beyond the standard model backgrounds, the first hints of supersymmetry would emerge. Studies such as the all-hadronic analysis in which I participated focus on a particular subset of the data where the most interesting signals should lie, in our case all-hadronic events passing certain energy and missing momentum thresholds. This analysis employed robust methods to accurately predict the standard model background rates directly from the collision data. Table A.1 shows the predicted standard model production rates and compares them to events

observed in the data. This table shows remarkable consistency between standard model background rates and observed data, with little to no excess of events. Hence, we observed no significant signs of supersymmetry in the 2011 data.

Table A.1: Predicted standard model backgrounds compared to observed 2011 data. The different search regions presented in the table impose successively higher cuts on both H_{T} (transverse momentum) and $\not{H}_{\mathrm{T}}$ (missing transverse momentum). No significant excess above standard model backgrounds is observed, and in some regions there are even slight deficiencies.

	Baseline ($H_{\mathrm{T}} > 350$ GeV/c) ($\not{H}_{\mathrm{T}} > 200$ GeV/c)	Medium ($H_{\mathrm{T}} > 500$ GeV/c) ($\not{H}_{\mathrm{T}} > 350$ GeV/c)	High H_{T} ($H_{\mathrm{T}} > 800$ GeV/c) ($\not{H}_{\mathrm{T}} > 200$ GeV/c)	High $\not{H}_{\mathrm{T}}$ ($H_{\mathrm{T}} > 800$ GeV/c) ($\not{H}_{\mathrm{T}} > 500$ GeV/c)
$Z \to \nu\bar{\nu}$ from γ + jets	$376 \pm 12 \pm 79$	$42.6 \pm 4.4 \pm 8.9$	$24.9 \pm 3.5 \pm 5.2$	$2.4 \pm 1.1 \pm 0.5$
$t\bar{t}/W \to e, \mu + X$	$244 \pm 20 \,^{+30}_{-31}$	$12.7 \pm 3.3 \pm 1.5$	$22.5 \pm 6.7 \,^{+3.0}_{-3.1}$	$0.8 \pm 0.8 \pm 0.1$
$t\bar{t}/W \to \tau_{\mathrm{h}} + X$	$263 \pm 8 \pm 7$	$17 \pm 2 \pm 0.7$	$18 \pm 2 \pm 0.5$	$0.73 \pm 0.73 \pm 0.04$
QCD	$31 \pm 35 \,^{+17}_{-6}$	$1.3 \pm 1.3 \,^{+0.6}_{-0.4}$	$13.5 \pm 4.1 \,^{+7.3}_{-4.3}$	$0.09 \pm 0.31 \,^{+0.05}_{-0.04}$
Total background	928 ± 103	73.9 ± 11.9	79.4 ± 12.2	4.6 ± 1.5
Observed in data	986	78	70	3

Without signs of supersymmetry present in the data, our analysis turned to the task of excluding certain mass ranges for CMSSM parameters. Within certain mass ranges of the $m_{1/2}$ and m_0 parameters, CMSSM predicts that an excess of events beyond the standard model backgrounds should be present in the data. Since we observed no excess, we were able to use CL_s statistical methods to exclude these parameter ranges at the 95% confidence level. The CL_s method is a tool widely used in limit-setting analyses done for the LHC experiments at CERN. This method uses the data to compute the probability of the "signal + background" $(s+b)$ hypothesis vs. the "background only" (b) hypothesis. It defines a test statistic as a likelihood ratio for a given experimental result X for these two hypotheses:

$$Q(X) = \frac{\mathcal{L}(X, s+b)}{\mathcal{L}(X, b)}. \tag{A.1}$$

Confidence levels CL_{s+b} and CL_b are calculated according to the probability distribution function for the appropriate hypothesis in relation to the test statistic (Q) and its observed value (Q_{obs}).

$$CL_{s+b} = P_{s+b}(Q \leq Q_{obs}) \tag{A.2}$$

$$CL_b = P_b(Q \leq Q_{obs}) \tag{A.3}$$

The final confidence variable is then defined to be

$$CL_s \equiv CL_{s+b}/CL_b. \tag{A.4}$$

This construction leads to the signal hypothesis being excluded at confidence level CL whenever

$$1 - CL_s \leq CL. \tag{A.5}$$

Using this CL_s method rather than the CL_{s+b} confidence level alone avoids certain problems that the latter can encounter in dealing with boundary fluctuations caused by imperfect background modeling [13, 14].

Applying these methods to a collection of points in the m_0–$m_{1/2}$ plane, we were able to observe contours in this plane below which our data excludes these key parameters, and these contours are displayed in Fig. 1.1. It should be noted that supersymmetry could turn out to take a much different form than CMSSM, and excluding CMSSM does not exclude all possible forms of supersymmetry. Probing the data for CMSSM does not exhaust our options for supersymmetry searches, but it does provide valuable insights into the implications in the data for one of supersymmetry's simpler formulations.

BIBLIOGRAPHY

[1] D. Griffiths, *Introduction to Elementary Particles*, 2nd ed. (Wiley-VCH, Weinheim, Germany, 2008).

[2] J. Beringer et al. (Particle Data Group), "Review of Particle Physics," Phys. Rev. D **86**, 010001 (2012).

[3] CMS Collaboration, "Search for supersymmetry in all-hadronic events with missing energy," CMS-PAS-SUS-11-004, CERN, Geneva, Switzerland, 2011.

[4] CMS Collaboration, "Search for New Physics in the Multijet and Missing Transverse Momentum Final State in Proton-Proton Collisions at $\sqrt{s} = 7$ TeV," Phys. Rev. Lett. **109**, 171803 (2012).

[5] V. Frigo, "LHC map in 3D," AC Collection. Legacy of AC. Pictures from 1992 to 2002, 1997.

[6] CMS Collaboration, "The CMS experiment at the CERN LHC," JINST **3**, S08004 (2008).

[7] CMS Collaboration, "Missing transverse energy performance of the CMS detector," JINST **6**, P09001 (2011).

[8] CMS Collaboration, "Search for New Physics with Jets and Missing Transverse Momentum in pp collisions at $\sqrt{s} = 7$ TeV," JHEP **08**, 155 (2011).

[9] CMS Collaboration, "Particle-Flow Event Reconstruction in CMS and Performance for Jets, Taus, and MET," CMS-PAS-PFT-09-001, CERN, Geneva, Switzerland, 2009.

[10] CMS Collaboration, "Technical Proposal for the Upgrade of the CMS detector through 2020," CERN-LHCC-2011-006, CMS-UG-TP-1, CERN, Geneva, Switzerland, 2011.

[11] CMS Collaboration, "CMS Technical Design Report for the Phase 1 Upgrade of the Hadron Calorimeter," CERN-LHCC-2012-015, CMS-TDR-10, CERN, Geneva, Switzerland, 2012.

[12] S. P. Martin, "A Supersymmetry Primer," hep-ph/9709356, 1997.

[13] A. L. Read, "Modified frequentist analysis of search results (the CL_s method)," CERN-OPEN-2000-205, 2000.

[14] A. L. Read, "Presentation of search results: the CL_s technique," Journal of Physics G: Nuclear and Particle Physics **28**, 2693 (2002).